Proceedings of
11th European Conference on Turbomachinery Fluid dynamics & Thermodynamics
ETC11, March 23-27, 2015, Madrid, Spain

APPLICATION OF ANALYTICAL NOISE MODELS USING NUMERICAL AND EXPERIMENTAL FAN DATA

M. Sturm[*]*, M. Sanjosé*[#]*, S. Moreau*[#] *and T. Carolus*[*]

[*]University of Siegen, Department of Fluid- and Thermodynamics, Paul-Bonatz-Str. 9-11, 57068 Siegen, Germany, michael.sturm@uni-siegen.de

[#]Mechanical Engineering, Université de Sherbrooke, 2500 Boulevard de l'Université, Sherbrooke QC J1K2R1, Canada, marlene.sanjose@USherbrooke.ca

ABSTRACT

In this study, both tonal and broadband analytical models for the prediction of fan noise based on low computational costs simulations or experimental data are applied and validated. Various inflow conditions are considered to verify the ability of the tonal noise model to reproduce the tendencies between the different cases. The tones predictions are in very good agreement when using the numerical input data. For the prediction based on the experimental data the reduction of the tones with the flow control devices is well captured and the frequency-dependent variation of the tones amplitude is reproduced. The broadband noise is well predicted by a trailing-edge noise model over a wide frequency range and confirms that the trailing edge noise is the main broadband noise source mechanism in case of isolated axial fans.

INTRODUCTION

Due to strict governmental restrictions and the increasing consideration of comfort factors the acoustic performance of fans, whose usage is subject of our everyday life, becomes more and more important. Although numerical methods are widely used in the design process of fans, the calculation of the acoustics of fans is still a challenging issue. Since the computational costs for direct accurate acoustic simulations are too high for industrial applications, the noise emission predictions are often based on empirical models and iterative, lengthy experimental measurements. In the present work, analytical models of noise specific mechanisms are investigated for a ducted low-speed axial fan. Such models require temporal averaged input data that can be obtained by unsteady Reynolds Averaged Navier-Stokes (URANS) simulations.

In case of isolated ducted axial fans, the major annoyances are the perceived overall noise level and its tonal content (subjective noise). The latter is generated by the fluctuating blade forces induced by an inlet distortion, and radiated at the blade passing frequency (BPF) and its harmonics. Large flow structures sucked into the fan section, can be accelerated and amplified near the blade leading edge and create a non-axisymmetric and time-varying incident velocity field to the rotor blade (Sturm and Carolus, 2013a). The large flow structures are related to any flow asymmetry and installation effects. Moreover, they may be unsteady and responsible for unsteadiness of the sound levels at the BPF (Sturm and Carolus, 2014).

In the present work, the inlet distortion generation mechanism and the associated tonal noise are experimentally investigated on a 5-blade low-speed axial fan installed in a cylindrical duct where a controlled pressure-rise is applied. The bell mouth ended-duct open in an anechoic wind-tunnel. The flow conditions inside the anechoic room yields a massive and slow flow recirculation that is responsible for the inlet distortion (Sturm and Carolus, 2013a). The tonal noise related to the upstream distortion can be strongly reduced using flow conditioners. Hot wire measurements of the inflow are conducted in a plane one diameter upstream the fan for three inflow conditions investigated. Unsteady SAS (Scale Adaptive Simulations) are performed to complement the experimental database

and provide input for an analytical software. Two inflow boundary conditions are investigated: a case of pure axial inflow and the free inflow case of the experiments is also achieved numerically by using the hot wire data.

The tonal content of the fan noise spectra is investigated using an analytical prediction tool OPTIBRUI that uses the analytical response of Amiet (1976b) for stacked flat plates to discretize the rotor blade geometry and the acoustic power upstream of the fan is obtained by using Goldstein's acoustic analogy (Goldstein, 1976). Several cases are considered for the analytical tonal model: the hot-wire measurements for the different inlet flow conditions and several extraction planes from the two numerical simulations, in particular the amplification effects of the distortion is investigated. The broadband component of the fan is thought to be the self-noise mechanism and is not affected by the flow conditioner (Sturm and Carolus, 2013b). Consequently, the model based on the generalized Amiet's model (Roger and Moreau, 2005; Rozenberg et al., 2010) with pressure fluctuations reconstructed according to Rozenberg's model (Rozenberg et al., 2012) is applied only on the results of the simulation with the disturbed inflow to predict the broadband noise of the fan.

The paper is organized as follows: in the methodology section the experimental configuration and the hot-wire measurements are first described, then the numerical parameters of the simulations and the analytical models and their specific inputs are finally presented. In the results section, the extraction from the numerical simulations is first analyzed, then the tonal prediction based on the numerical and experimental data are compared with the experimental sound power levels. Finally the trailing-edge noise predictions are compared with the acoustic measurements.

METHODOLOGY

Experimental Configuration

In this study the standardized test rig for acoustic measurements of fans at the University of Siegen is used. This test rig has been used in several studies (Sturm and Carolus, 2013a,b), and hence only the main features are repeated here. The fan takes air from a large anechoic room and exhausts into a duct with an anechoic termination. The flow inlet is located off-center in the reverberant floor. The low pressure fan unit contains five cambered and swept blades which are designed with an in-house design software for axial fans. The rotor of diameter d_2 is manufactured with a production tolerance of at least 0.1 mm and balanced with very high precision (at least G6.3 according to (DIN ISO 1940-1)) to avoid any non-aeroacoustic sound sources. A bell mouth type inlet nozzle with a $1/4$ rotor diameter radius is employed. Thin supporting struts are positioned one rotor diameter downstream of the rotor. No other obstructions are present.

The acoustic measurements are conducted by using three free-field microphones (Bruel & Kjaer type 4190) with a radial distance of 1.3 m from the leading edge of the rotor, an angular spacing of 35° from the axis of rotation and 1.35 m above ground. The signals are recorded with a sampling frequency of $f_s = 25.6$ kHz for an acquisition time of 10 s. The evaluated sound power spectra are an average of the three microphones with a frequency resolution of $\Delta f = 1$ Hz:

$$SWL(f) = 10\log\left(\frac{1}{3}\sum 10^{0.1\cdot L_{p,i}(f)}\right) + 10\log\frac{A_M}{A_0} + 10\log\frac{(\rho a)_0}{\rho a} \tag{1}$$

where $L_{p,i}$ are the measured sound pressure levels at the three microphone positions, $A_M = 2\pi r^2$ is the measurement surface, $A_0 = 1\ m^2$ the reference area and $(\rho a)_0 = 400\ kg/m^2 s$ the characteristic acoustic impedance. For details of the sound power estimation, see (Carolus et al., 2015). All measurements were performed at a rotational speed of $n = 3000$ rev/min and at the fan design operating flow rate coefficient $\phi_{design} = 0.195$. The uncertainty is less than $2\ \%$ for aerodynamic measurements or less than 2 dB for acoustic measurements respectively, see (Carolus et al., 2015).

The application of two inflow conditioners as shown in Fig. 1, allows the investigation of the tonal noise related to the inflow distortion. The Hemispherical Flow Conditioner (HFC) consists of

a combination of a fluid conditioner structure, which reduces the lateral turbulence, and a downstream layer of wire mesh to reduce axial disturbances (Scheimann and Brooks, 1980). A second inflow conditioner is a plane layer of small tubes, inserted into the duct upstream of the fan (Tubular Flow Conditioner, TFC). The axial position of the TFC with respect to the rotor is shown in Fig. 2. Geometric details of the flow conditioners have been described by Sturm and Carolus (2013b).

(a) Tubular Flow Conditionner (TFC). (b) Hemispherical Flow Conditionner (HFC).

Figure 1: Inflow conditioners.

To capture spatial variations of the flow field in the intake a cross section of the duct one fan diameter upstream of the leading edge is scanned by a 3D hot-wire probe. The anemometer operates in a constant-temperature mode. The measured signals are temperature corrected by using a temperature probe. The hot-wire probe is calibrated in a low turbulence wind tunnel.

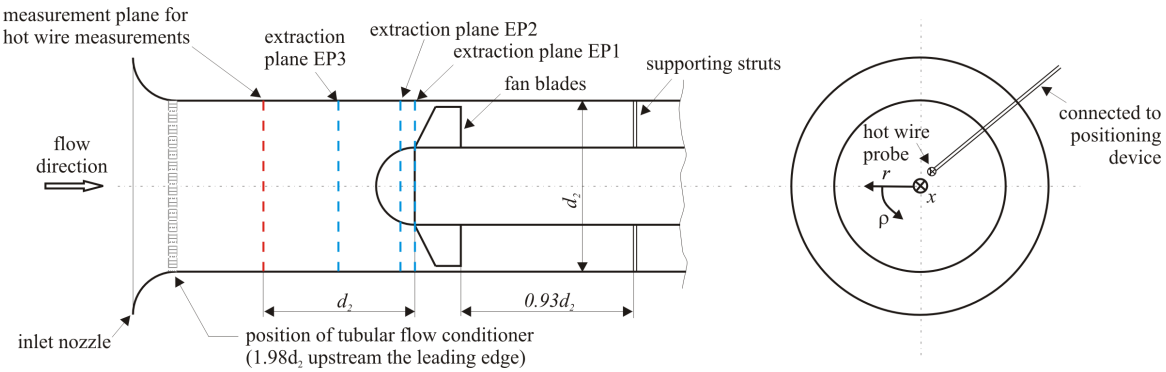

Figure 2: Lateral view of the axial fan section (left) and top view (right).

The orientation of the polar coordinate system for the hot wire measurements is indicated in Fig. 2 (right). The probe is attached to an automatic two axis positioning system, which is able to move the probe in circumferential and radial direction without disturbing the flow inside the duct. The device has a positioning accuracy of 0.02 mm and 0.15°. The uniformly arranged measurement points in the cross sectional plane of the duct have an angular distance of $\Delta\varphi = 5°$ and radial distance of $\Delta r = 5\,\text{mm}$, respectively. Together with the center of the plane, this leads to 2017 measurement points. All measurements are conducted over a time interval of two seconds with a sampling rate of $f_s = 25.6\,\text{kHz}$.

The inflow velocity profiles are evaluated in terms of the axial velocity c_m, the circumferential velocity c_u and the radial velocity c_r, according to the coordinate system indicated in Fig. 2. Due to the fact that the data of the hot wire measurements are not recorded simultaneously at the different measurement points, only time averaged data is evaluated assuming a statistically stationary state and used as a stationary inlet boundary condition for the simulations. All velocity components are made non-dimensional by the volumetric averaged velocity c_{vol} inside the duct.

Numerical Simulations

For the numerical simulations the fan section, as depicted in Fig. 2, is modeled using the commercial meshing tool ANSYS IcemCFD. As shown in Fig. 3, the computational domain includes the ducted fan with the hub and is divided into three subdomains, where the rotating rotor domain is separated by sliding mesh interfaces from the stationary subdomains. The inlet is located one fan diameter upstream of the leading edge, while the outlet is placed two diameter downstream the trailing edge. The small tip gap of $s/d_2 = 0.1\,\%$ is fully resolved by the numerical mesh. The unstructured mesh consists of 21.4 million cells including 5 prism layers with a $10\,\%$ growth rate at walls and refined regions in the vicinity of the blades. The dimensionless wall distance on the blades is $y^+_{avg} = 4$ ($y^+_{min} = 0.38$, $y^+_{max} = 29.8$).

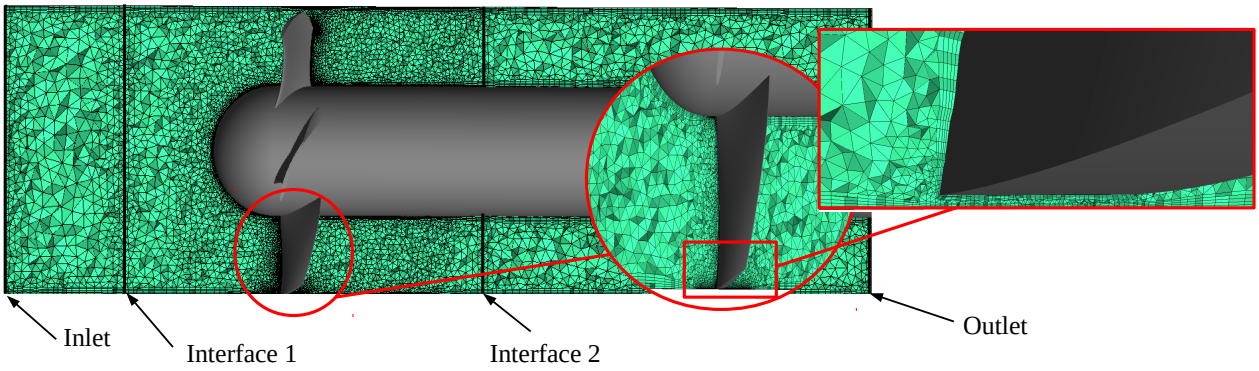

Figure 3: Computational domain and numerical mesh of the simulated fan section.

The pressure outlet boundary condition is set to a gauge pressure of $0\,$Pa. Two cases, which differ only in the inlet boundary condition are investigated: (i) a pure axial, undisturbed inflow achieved by a constant inlet velocity according to the design flow rate and (ii) a disturbed inflow where the velocity data of the hot wire measurements is used for the inlet boundary condition. While the latter are the real inflow conditions, the former represents an ideal inflow condition which can be achieved only numerically.

The simulations are conducted using the commercial solver ANSYS Fluent 14.5.7. Although time averaged simulation results are sufficient for the application of the presented noise models, the SAS approach is chosen to obtain instantaneous data which can be compared with intermediate results of the acoustic models like the spectra of the blade pressure fluctuations. All quantities are solved using second order schemes. The SIMPLEC algorithm is used to solve the pressure-velocity coupling. The time step is 5×10^{-6}s, which leads to a resolution of 4000 time steps per blade-passage. The input data for the tonal noise model is extracted at three different planes shown in Fig. 2: extraction plane EP1 at the leading edge, extraction plane EP2 one quarter chord length upstream of the leading edge and extraction plane EP3 midway between the leading edge and the interface upstream of the rotor.

Tonal and Broadband Noise Models

This section presents the tonal and broadband analytical models used for the acoustic predictions and comparison with experimental measurements. These models are integrated in the OPTIBRUI software for noise prediction of axial turbomachinery developed at Université de Sherbrooke. The geometrical modeling of the fan is identical for the two noise mechanisms. The fan is mounted in an annular duct of constant section. The cylindrical reference frame $\mathcal{R}_d(r_d, \theta_d, z_d)$ is fixed to the duct with its axial direction corresponding to the machine axis oriented towards the exhaust of the duct. In order to account for the complex blade geometry, the blade is split into several annular strips of identical span dr. At each strip r_d, the blade element is described as a flat plate of constant chord $C\,(r_d)$ and stagger angle $\chi\,(r_d)$. The radial stacking of the blade elements is parametrized by the lean

and sweep angles ($\varphi_{LE}(r_d)$,$\psi_{LE}(r_d)$) that define the positioning of the blade element leading-edge with respect to a rotational and a meridional plane crossing the blade leading-edge at the hub. Similar angles at the trailing-edge ($\varphi_{TE}(r_d)$,$\psi_{TE}(r_d)$) can be deduced from the chord and stagger parameters. Each annular strip can be unwrapped into a rectilinear cascade geometry. A local Cartesian reference frame $\mathcal{R}_c(x_c, y_c, z_c)$ is defined to compute the blade element acoustic response. The (O, x_c) direction is aligned with the flat plate pointing downwards, the (O, y_c) direction is normal to the blade element and the (O, z_c) is aligned with either the leading or the trailing edge of the blade element depending whether a noise mechanism at the leading or the trailing edge is computed and is pointing towards the tip of the blade. The matrix from the coordinate system $\mathcal{R}_c$ to the coordinate system $\mathcal{R}_d$ is written Q. Hanson (Hanson, 2001) provides the transfer matrix from $\mathcal{R}_d$ to $\mathcal{R}_c$ that includes three successive rotations of angle α, θ and β related to the lean, sweep and stagger angles of the blade element.

Tonal noise model with in-duct propagation

The rotor is assumed to be located in an infinite annular duct with a constant section and rigid walls. For the acoustic propagation, only an inviscid mean axial flow of Mach number M_a is considered. Within these assumptions, the Goldstein's analogy (Goldstein, 1976) provides the acoustic pressure in the duct resulting from the force $\vec{f}$ exerted by the blade surface S on the fluid using the annular duct Green's function G:

$$p(\vec{x}, t) = \int_{-T}^{T} \iint_{S} \frac{\partial G\left(\vec{x}, t|\vec{x_0}, t_0\right)}{\partial x_{0,i}} \, f_i\left(\vec{x_0}, t_0\right) dS\left(\vec{x}_0\right) dt_0 \tag{2}$$

with t_0 and t the emission and observer times and $\vec{x}_0$ and $\vec{x}$ the emission and observer positions respectively in the duct coordinate system.

The Green's function can be written on the duct mode basis using the indices n and j for the circumferential and radial modes respectively in the frequency space:

$$G\left(\vec{x}, t|\vec{x_0}, t_0\right) = \frac{\mathbf{i}}{4\pi} \sum_{n=-\infty}^{+\infty} \sum_{j=0}^{+\infty} \frac{E_{nj}(r_0)\, E_{nj}(r)\, e^{\mathbf{i}n(\theta-\theta_0)}}{\Gamma_{nj}} \int_{-\infty}^{\infty} \frac{e^{-\mathbf{i}\left(\gamma_{nj}^{\pm}(x-x_0)+\omega(t-t_0)\right)}}{\kappa_{nj}} d\omega \tag{3}$$

with $k_0 = \omega/c_0$, E_{nj} the duct radial function depending on the eigenvalue χ_{nj} of norm $\Gamma_{nj}/2\pi$, $\gamma_{nj}^{\pm} = \frac{M_a k_0 \pm \kappa_{nj}}{\beta^2}$ the axial acoustic wavenumber and $\kappa_{nj}^2 = k_0^2 - \beta^2\chi_{nj}^2$ the cut-off criteria. The superscript $\pm$ is related to the direction of propagation for $z > z_0$ and $z < z_0$, respectively.

The force can be related to the pressure jump across the blade: $\vec{f} = \Delta P \vec{n}$ with $\vec{n} = \text{sign}\,(\Omega)\, \vec{e}_{y,c}$ the local normal of the blade. Assuming identical blades uniformly distributed, the pressure jump is identical for each blade but delayed in time by $\frac{2\pi(j-1)}{\Omega B}$ for the j^{th} blade and can be decomposed into a Fourier series to account for the rotational periodicity. The Fourier coefficient of the p harmonics is written $\Delta P(\vec{x_0}, t_0)$.

A change of reference frame is required to exchange the integration order by integrating over a fixed surface. For $T \to \infty$ and uniformly distributed blades, the acoustic pressure becomes the summation of tones. The acoustic pressure at the harmonic frequency $sB\Omega$ is:

$$\widehat{p}^{\pm}\left(r_d, \theta_d, z_d, t\right) = \sum_{n=-\infty}^{+\infty} \sum_{j=0}^{+\infty} E_{nj}(r)\, e^{\mathbf{i}\left(n\theta - \gamma_{nj}^{\pm} z_d\right)} P_{nj,sB-n}^{\pm} e^{-\mathbf{i}sB\Omega t} \tag{4}$$

The modal coefficient can be computed by splitting the surface integration first along the circumferential extent of the blade and then along its span:

$$\begin{aligned} P_{nj,sB-n}^{\pm} \;=\; & \frac{-\text{sign}\,(\Omega)\, B}{2\pi\Gamma_{nj}\kappa_{nj}} \int_{R_H}^{R_T} \left\{ -\mathbf{i}Q_{23}\frac{\partial}{\partial r_0} - \frac{n}{r_0}Q_{22} + \gamma_{nj}^{\pm}Q_{21} \right\} E_{nj}\left(r_0\right) \\ & \times e^{\mathbf{i}\left(\gamma_{nj}^{\pm} z_{d,LE}(r_0) - n\theta_{d,LE}(r_0)\right)} I_{nj,sB-n}^{\pm} dr_0 \end{aligned} \tag{5}$$

with $(x_{d,LE}, y_{d,LE}, z_{d,LE})$ the coordinates of the leading-edge and $I^{\pm}_{nj}$ the chordwise integral of the pressure jump. The hub-to-tip spanwise integration in Eq. (5) is replaced by a discrete summation over the annular strips of the blade. The chordwise integral $I^{\pm}_{nj}$ is approximated assuming a chordwise wavenumber without sweep or lean effects. Following the acoustic response for an isolated flat plate of Patterson and Amiet (1976), the pressure jump chordwise integral can be computed analytically and related to the harmonics of the incident upwash velocity gust $\widehat{w}_p$ on the leading-edge considering:

$$I^{\pm}_{nj,sB-n} = \frac{C}{2r_0}\int_0^2 \widehat{\Delta P}_{sB-n}(x_c^*)\, e^{\mathbf{i}\frac{c}{2}\left(\frac{n}{r_0}\sin\chi+\gamma^{\pm}_{nj}\cos\chi\right)x_c^*} dx_c^* = 2\pi\rho_0 W \widehat{w}_{sB-n}\left(\mathcal{L}^1_{nj}+\mathcal{L}^2_{nj}\right) \tag{6}$$

with W the relative velocity and $\mathcal{L}^1_{nj}$ and $\mathcal{L}^2_{nj}$ the blade response and the back-scattering of the trailing-edge respectively for supercritical gusts defined in (Reboul, 2010).

Finally the acoustic power is obtained by considering only the cut-on modes that fulfill $\kappa^2_{nj} > 0$ (Meyer and Envia, 1996):

$$\Pi^{\pm}_s = \sum_{n=-\infty}^{+\infty}\sum_{j=-\infty}^{+\infty} \frac{\Gamma_{nj}\,\beta^4\,k_{0,s}\,\kappa_{nj}}{\rho_0 c_0\left(k_{0,s}\pm M_a\kappa_{nj}\right)^2}|P^{\pm}_{nj,sB-n}|^2 \tag{7}$$

The acoustic power measured upstream of the fan is directly compared to the Π^-_s estimation.

Broadband noise with free-field propagation

For the case of broadband self-noise model, the acoustic propagation is computed in free-field following the extension of Amiet's theory (Roger and Moreau, 2005) applied for each uncorrelated blade strip (Moreau and Roger, 2007; Guedel et al., 2009). The radiated sound field is calculated by integrating the induced surface sources on the actual chord length, C and the strip span, dr, assuming convection of frozen turbulent boundary-layer eddies past the trailing edge. In the assumption of large aspect ratio dr/C, the spectral density of the sound pressure in the far field is obtained using:

$$S_{pp}(\vec{x}_c,\omega) \;=\; \left(\frac{\omega C y_c}{2\pi c_0 S_0^2}\right)^2 \frac{dr}{2}\left|\mathcal{L}\left(\frac{\omega}{U_c},\frac{\bar{k}z_c}{S_0}\right)\right|^2 \Phi_{pp}(\omega) l_z(\omega) \tag{8}$$

where $\mathcal{L}$ is the aeroacoustic transfer function, derived analytically (Amiet, 1976a), and taking into account leading-edge back-scattering, supercritic and subcritic gusts (Roger and Moreau, 2005).

$\Phi_{pp}(\omega)$ is the wall-pressure spectrum upstream of the trailing-edge that has to be reconstructed from the RANS or URANS simulation or directly extracted in the case of the SAS while $l_z(\omega)$ is the corresponding spanwise correlation length described by Corcos' model.

In case of rotation, the far-field sound pressure level of a low solidity fan with B uncorrelated blades is given by an integration over all possible circumferential positions of the single airfoil formulation Eq. (8) (Paterson and Amiet, 1979):

$$S_{pp}(\vec{x},\omega) = \frac{B}{2\pi}\int_0^{2\pi}\left(\frac{\omega_e(\Psi)}{\omega}\right)^2 S^{\Psi}_{pp}(\vec{x}_c,\omega_e)d\Psi. \tag{9}$$

The factor $\omega_e(\Psi)/\omega$ accounts for Doppler effects due to the rotation (Sinayoko et al., 2012). The acoustic power measured upstream of the fan is directly compared to the sound power estimated by the integration of Eq. (9) over a hemisphere centered on the fan and looking towards inlet:

$$\Pi^-(\omega) \;=\; \frac{2\pi R^2}{\rho c_0}\int_{\pi/2}^{\pi} S_{pp}(R,\Theta,\omega)d\Theta \tag{10}$$

with R and Θ the spherical distance and polar angle of the observers measured from the fan center and machine axis (O, z_d).

The wall-pressure spectrum upstream of the trailing-edge is obtained by using Rozenberg's spectral model (Rozenberg et al., 2010, 2012) which is developed for attached turbulent boundary layer with adverse pressure gradient and accounts for Reynolds-number effects. This model is based on several characteristic parameters of the boundary layer. For each strip centerline at the extraction point close to the trailing-edge on the suction, an extraction coordinate system is built $(\vec{x}_t, \vec{y}_n, \vec{e}_r)$ along the tangential, normal directions to the suction side of the mid-strip profile and the radial direction of the cylindrical coordinate system, respectively. The quantities are extracted from a phase-averaged snapshot (over a fan revolution) of the SAS simulation for the five blades and averaged. The relative velocity magnitude w and the relative total pressure are extracted along the $\vec{y}_n$ direction. As the flow is incompressible, the boundary layer thickness δ_{99} is determined by the height where the total pressure recovers the exterior constant value. Then the velocity profile is integrated to obtained the displacement δ^* and momentum θ thicknesses. The Rozenberg's model requires also the maximum value of the normal shear-stress $\tau_M = \max_{0<y_n<\delta} \left[\mu \frac{\partial w}{\partial y_n}\right]$ along the extraction line. The wall pressure gradient along the strip centerline $\frac{\partial p}{\partial x_t}$ is computed at the same extraction position. For the Corcos's model the convective velocity is determined as 80% of the exterior velocity $U_e = w\,(y_n = \delta_{99})$.

RESULTS

Parametric Study of the excitation of the fan

The main input of the tonal noise mechanism is the relative velocity distortion seen by the leading edge. Along the simulation, the instantaneous velocity is extracted in three planes shown in Fig. 2. As can be observed in Fig. 4(a), the instantaneous velocity field is strongly influenced by the rotor potential field, even in the plane EP2 or EP3. Such velocity would generate high and unphysical harmonic at the blade rotation harmonic. To avoid this spurious effect, the potential effect of the rotor must be removed. The velocity is therefore averaged in the duct reference frame. A preliminary study has shown than 20 instantaneous fields to cover each blade passage period were sufficient to successfully remove the potential effect. The averaged field over a blade passage for the disturbed simulation is clearly non-axisymmetric as shown in Fig. 4(b).

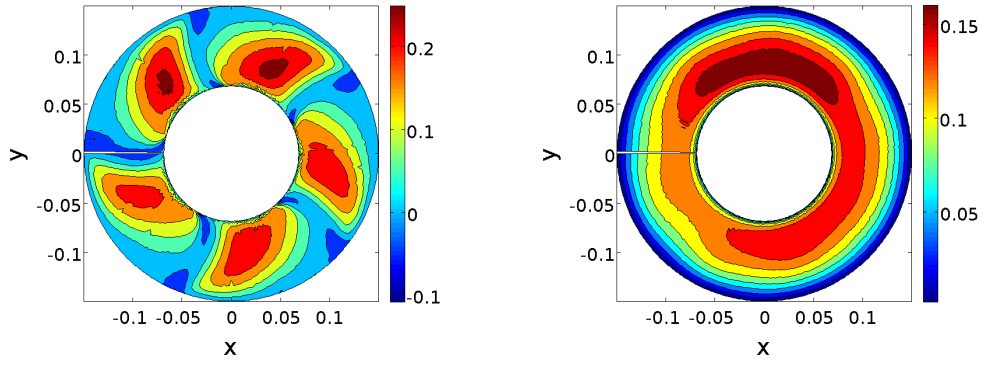

(a) Instantaneous flow field.

(b) Flow field averaged over one blade passage in the duct reference frame

Figure 4: Dimensionless azimuthal component of the absolute velocity in the EP1 plane for the disturbed case.

Seven blade passages have been extracted once the blade force components have reached a stationary state. The Fourier coefficients of the upwash components of the relative velocity at mid span of the blade in the EP2 extraction plane are given in Fig. 5 for the disturbed and undisturbed simulations. The coefficient amplitudes are 10 times higher in the disturbed simulation than in the undisturbed one. Also, some variations can be observed between the successive blade passage periods

of averaging. The interpolation procedure induces some errors yielding a remaining fluctuation level of 5×10^{-5} for the higher harmonics. However, some distinct fluctuations for the lower harmonics remain in case of the disturbed inflow. The upwash velocity for the center strip is shown in Fig. 6(a) for the disturbed and undisturbed simulations. The interpolated values obtained after the averaging process show point to point variations that highlights the interpolation errors. These oscillations are responsible for the non zero levels at high harmonics. Still, after smoothing with a low pass filter, the undisturbed case show some large scale oscillations. These oscillations are responsible for the low harmonics levels observed in Fig. 5(b). The remaining oscillations in case of the undisturbed may be a numerical consequence of the mesh non-homogeneity close to the leading edge as shown in Fig. 6(b) for the extraction plane. Since the same mesh was used for both simulations, these mesh-induced oscillations should be also present in case of the disturbed case. However, it is clearly visible from Fig. 6(a) that the oscillations in case of the disturbed inflow are much stronger which can only be related to coherent structures emerging from the disturbed inflow.

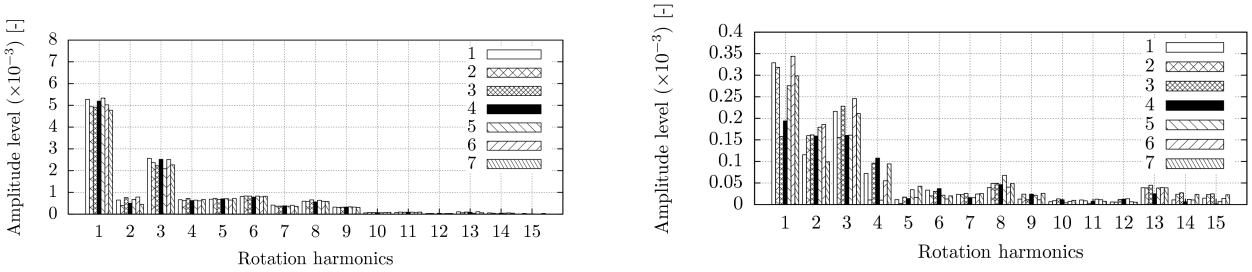

(a) Disturbed case.

(b) Undisturbed case.

Figure 5: Fourier coefficients of the upwash component of the dimensionless relative velocity at the mid-span of the blade in EP2. Seven successive blade passage periods are shown with different patterns.

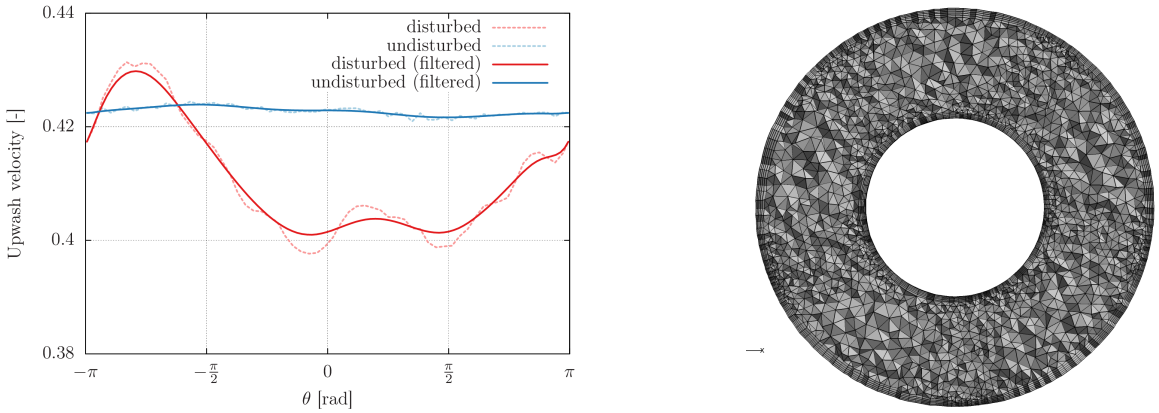

(a) Upwash velocity fluctuations for the disturbed and undisturbed simulations in EP2 location. Light dash lines: interpolated values used in the analytical computation, dark plain lines: low pass filtered values.

(b) Mesh view at the EP2 mesh location.

Figure 6: Upwash velocity extractions in EP2 mesh location.

Tonal Noise Prediction based on Numerical Simulation

The tonal noise predictions computed for the first blade passage period distortion are compared with the experimental measurements in Fig. 7. The predictions obtained from the three extraction

planes reflect the tendencies observed in the experiments. At BPF the agreement of the prediction for EP1 is within 1 dB, while it is up to 5 dB for higher harmonics. Comparing the different inflow conditions the level of the BPF tone reduction of 10 dB is similar to the experimental reduction obtained with the HFC inflow device. The extractions made in EP3 upstream of the annular section provide the higher tone levels. The initial disturbances observed in EP3 are diminished as they are propagated downstream. This could be due to either numerical dissipation or related to the extra distortion caused by the bulk-head that is not present in EP3.

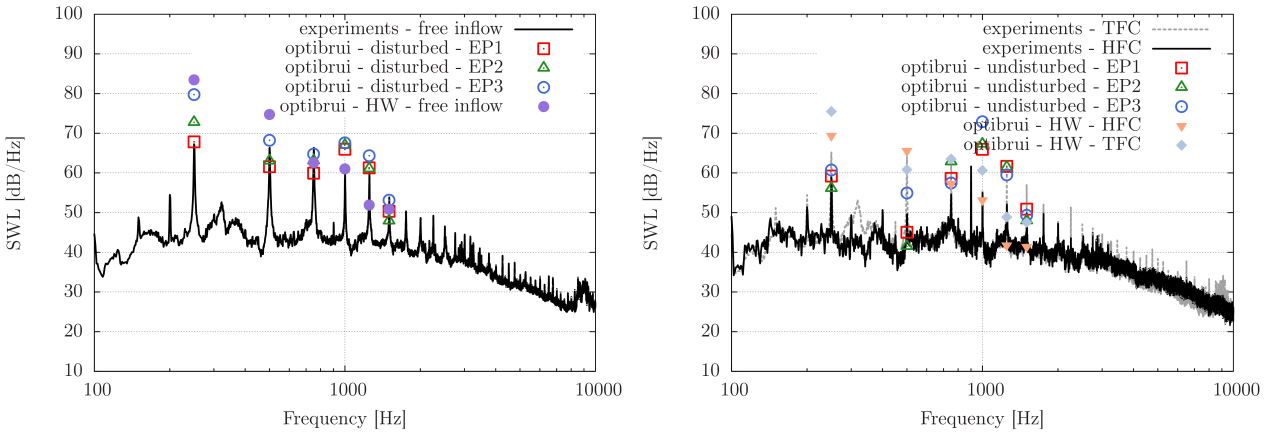

(a) Disturbed case.

(b) Undisturbed case.

Figure 7: Comparison of the acoustic prediction from the tonal model based on numerical simulations with experimental measurements upstream of the duct intake.

The tonal noise prediction based on the seven successive blade passage periods that have been extracted are shown in Fig. 8. As observed in the experiments the harmonics levels are fluctuating from one blade passage period to another. The levels of fluctuations are increasing for extraction planes closer to the blade leading-edge. The captured fluctuations might be related to secondary flow and strong unsteadiness captured close to fan blade by the SAS turbulent model.

Tonal Noise Prediction based on Hot-Wire measurements

The hot-wire measurements recorded one duct diameter upstream of the fan for the three inflow conditions can also be used as distortion input in the analytical model. To account for the duct contraction yielding flow acceleration and pre-swirl effects an amplification factor is computed for each relative velocity components by evaluating the ratios of the velocity components between the inlet plane and the EP1 plane. The velocity is averaged in the duct reference frame over a fan rotation to remove any potential effects that could affect the calculation of the amplification. The calculation considers only the annular area between the hub and the shroud and is an azimuthal average. The radial, azimuthal and axial components of the amplification factor are shown in Fig. 9. A smoothing of the hot-wire measurements was required to avoid unphysical high tones related to point to point variations in the measurements. The acoustic predictions are shown in Fig. 7 with the filled symbols. As for the predictions based on the numerical results extracted in EP3 plane the tones are higher than the measured ones. This is attesting that the upwash velocity fluctuations are damped while there are convected towards the fan. The reduction of the tones with the flow control devices is well captured. Except for the second harmonics, the HFC input data yields a prediction of tonal noise lower than the TFC one, showing that the former provides cleaner inflow conditions.

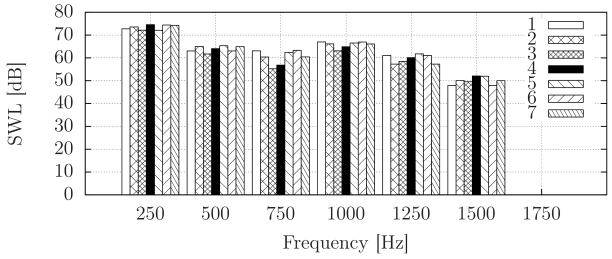

(a) Disturbed case.

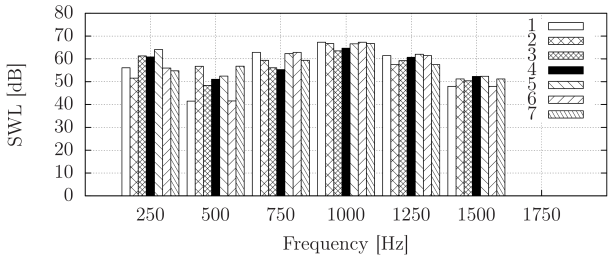

(b) Undisturbed case.

Figure 8: Acoustic predictions from the tonal noise model for seven successive blade passage velocity fields extracted at the EP2 location.

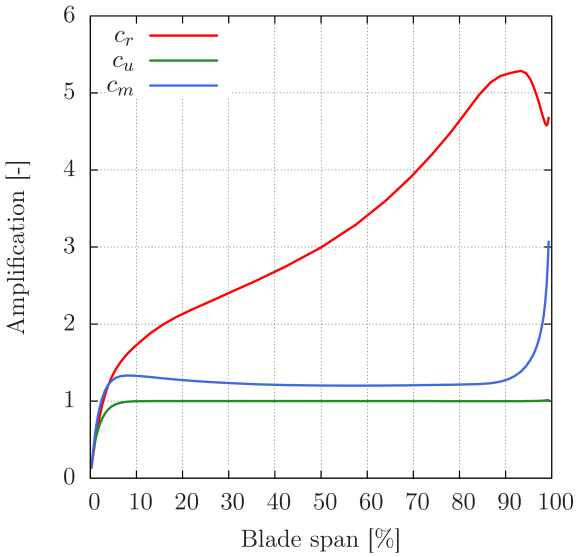

Figure 9: Amplification factor for the radial, circumferential and axial velocity component c_r, c_u and c_m.

Broadband Noise Prediction based on Numerical Simulation

For the trailing-edge noise model, the input data are extracted from an instantaneous field of the disturbed simulation at the five blade strip locations close upstream of the trailing-edge. The flow topology is shown in Fig. 10 where the trailing-edge is on the left hand side. The streaklines allow identifying a large flow detachment at the hub and a small one near the trailing-edge at the tip. At mid span the shear-stress lines are well aligned and parallel identifying a well attached boundary layer. According to the pressure contours, higher pressure gradients are found on the upper part of the blade span. The data are extracted for the five strips on the suction-side at 95% of the chord, following the extraction procedure described in the methodology section. The extraction points are shown by the purple spheres in Fig. 10. The acoustic predictions are compared with the experimental spectra in Fig. 11. The contribution to the noise from each strip is also provided. Because of the flow detachment the acoustic contribution from the first strip has a higher roll-off slope. Surprisingly, the second strip has a larger contribution at low frequency than the other strips, probably a consequence of the flow deflection coming from the hub recirculation. Indeed, the analysis of the extractions in Fig. 12 shows the singularity of the second strip: with high boundary layer tickness and strong shear-stress. The location of the second strip extraction point in Fig. 10 is right in the continuation of hub corner vortex imprint on the surface, affecting the beneath boundary layer. Finally the total spectrum is within 3 dB agreement of the broadband noise level captured in the experiments, except above 8 kHz where motor drive additional noise could explain the higher levels in the experiments.

CONCLUSIONS

Unsteady numerical simulations have been performed using the SAS turbulent model on a 5-blade low-speed axial fan in a duct for which several flow and acoustic measurements have been performed. Inflow conditioners have shown to play a important reduction effect of the tonal noise. Two cases for the simulation have been considered to mimic the effect of the flow conditioners at the duct inlet. An undisturbed simulation using a uniform axial velocity inlet condition reproduces the hemispherical flow conditioner (HFC) experimental case. A disturbed simulation reproduces the free inflow condition. The inlet profiles are radial, circumferential and axial velocity maps that have been measured

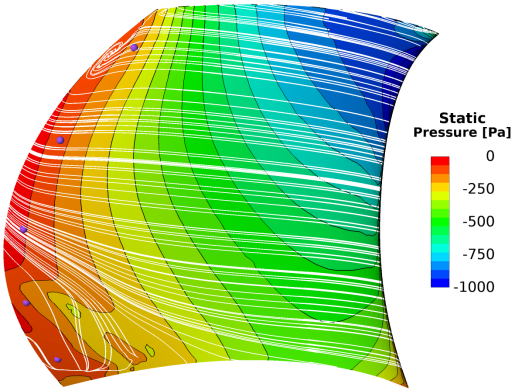

Figure 10: Visualization of the flow topology on the blade. The static pressure is shown with color contours and the streaklines are shown with the white lines. Purple dots show the extraction locations.

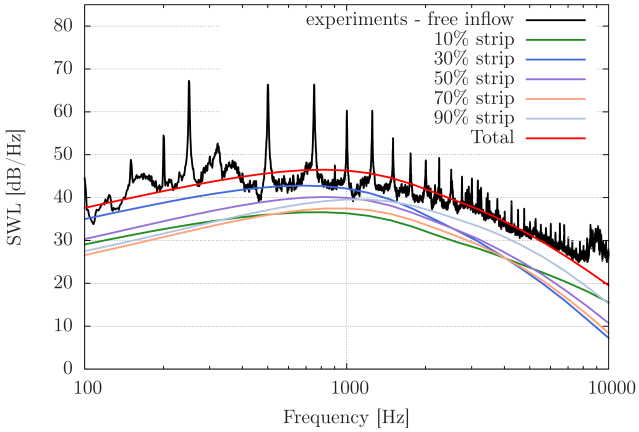

Figure 11: Comparison of the acoustic prediction from the trailing-edge noise model with experimental measurements upstream of the duct intake. The total noise spectra as well as the contributions from the 5 blade strips is provided. From left to right: boundary layer thicknesses, exterior stream velocity, pressure gradient, normal shear-stress.

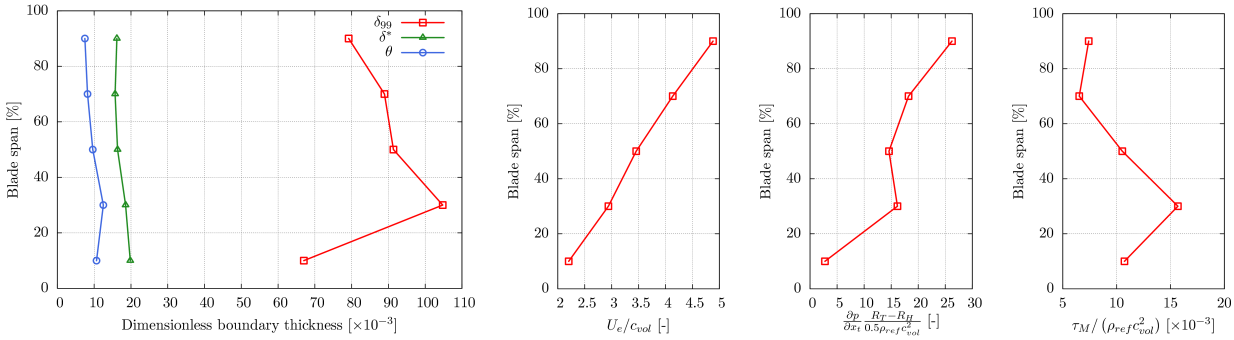

Figure 12: Boundary layer extractions along the blade strip.

downstream of the bell-mouth using a rotating hot-wire test rig. Analytical tonal and broadband noise prediction available in the OPTIBRUI software have been computed using data extracted from both simulations. The input for the tonal noise are the relative velocity maps upstream of the fan. An averaging procedure in the duct reference frame allows removing the potential effect of the rotor on the velocity components. The tone predictions for both the disturbed and undisturbed cases are in very good agreement with the free and HFC inflow experiments. Although certain differences for the different extraction planes can be observed when the distortion is present, the reduction of the source mechanism as well as the relative influence of the first three harmonics is captured and independent of the position of the extraction planes. Data extracted upstream of the bulk head provide tone levels 5 dB above the predictions from data extracted in the annular section. This reveals that the distortion is damped while propagating towards the fan. Assuming a quasi-steady evolution and using extractions from successive blade passage periods, fluctuations of the tone levels have been captured as identified in the experiments. Finally the analytical trailing-edge model has been applied to predict the broadband noise component of the acoustic spectra. The wall-pressure spectra is reconstructed from boundary flow data extracted close to the trailing-edge. The wall-pressure spectra model accounts for the Reynolds effects and the adverse pressure that develops along the chord. The acoustic model provides a good agreement with the broadband noise level in the measurements. The contributions

from each strip can be related to the flow topology of the boundary layer on the blade suction side demonstrating the relevance of the wall-pressure spectra model.

ACKNOWLEDGEMENTS

Computations were made on the supercomputer Mammoth-MS2 from Université de Sherbrooke, managed by Calcul Québec and Compute Canada. The operation of this supercomputer is funded by the CFI, NanoQuébec, RMGA and FRQ-NT. M. Sanjosé and S. Moreau would like to acknowledge Airbus, Safran and Valeo partners of the aeroacoustic industrial Chair of the Université de Sherbrooke funding this research project. M. Sturm and T. Carolus gratefully acknowledge the funding by the "Deutsche Forschungsgemeinschaft (DFG)".

REFERENCES

R. K. Amiet. Noise due to Turbulent Flow past a Trailing-Edge. *J. Sound Vib.*, 47(3):387–393, 1976a.

R. K. Amiet. High frequency thin-airfoil theory for subsonic flow. *AIAA J.*, 14(8):1076–1082, 1976b.

T. Carolus, T. Zhu, and M. Sturm. A Low Pressure Axial Fan for Benchmarking Prediction Methods For Aerodynamic Performance and Sound. In *FAN2015 - International Conference on Fan Noise, Technology and Numerical Methods*, Lyon, France, April 2015.

DIN ISO 1940-1. Mechanical vibration - Balance quality requirements for rotors in a constant (rigid) state - Part 1: Specification and verification of balance tolerances, 2004.

M. E. Goldstein. *Aeroacoustics*. McGraw-Hill, Inc, 1976.

A. Guedel, Y. Rozenberg, M. Roger, and G. Perrin. Experimental validation of a model of fan trailing-edge noise. *Noise Control Eng J.*, 57(4):318–326, 2009.

D. B. Hanson. Theory for broadband noise of rotor and stator cascades with inhomogeneous inflow turbulence including effects of lean and sweep. Technical report, NASA, 2001.

H. D. Meyer and E. Envia. Aeroacoustic analysis of turbofan noise generation. Technical report, NASA, 1996.

S. Moreau and M. Roger. Competing Broadband Noise Mechanisms in Low-Speed Axial Fans. *AIAA J.*, 45(1):48–57, 2007. doi: 10.2514/1.14583.

R. W. Paterson and R. K. Amiet. Noise of a model helipcopter rotor due to ingestion of turbulence. Technical Report CR 3213, NASA, 1979.

R. W. Patterson and R. K. Amiet. Acoustic radiation and surface pressure characteristics of an airfoil due to incident turbulence. Technical report, NASA, 1976.

G. Reboul. *Modélisation du bruit à large bande de soufflantes de turboréacteurs*. PhD thesis, Ecole Centrale de Lyon, 2010.

M. Roger and S. Moreau. Back-scattering correction and further extensions of Amiet's trailing-edge noise model. Part 1: theory. *J. Sound Vib.*, 286(3):477–506, 2005.

Y. Rozenberg, M. Roger, and S. Moreau. Rotating Blade Trailing-Edge Noise: Experimental Validation of Analytical Model. *AIAA J.*, 48(5):951–962, 2010.

Y. Rozenberg, G. Robert, and S. Moreau. Spectral model accounting for pressure gradient and Reynolds effects for the prediction of trailing-edge noise using RANS simulations. *AIAA J.*, 50 (10):2168–2179, 2012.

J. Scheimann and J. D. Brooks. A Comparison of Experimental and Theoretical Turbulence Reduction from Screens, Honeycomb and Honeycomb-Screen Combinations. *11th Aerodynamic Testing Conference, Colorado Springs, USA, AIAA, Technical Papers*, pages 129–137, 1980.

S. Sinayoko, M. Kingan, and A. Agarwal. Trailing edge noise prediction for rotating blades: analysis and comparison of two classical approaches. In *18th AIAA/CEAS Aeroacoustics Conference*, AIAA Paper 2012-2302, Colorado Springs, CO, USA, June 2012.

M. Sturm and T. Carolus. Impact of the large-scale environment on the tonal noise of axial fans. *Proc. Inst. Mech. Eng., Part A: J. Power Energy*, 227(6):703–710, 2013a.

M. Sturm and T. Carolus. Large Scale Inflow Distortions as a Source Mechanism for Discrete Frequency Sound from Isolated Axial Fans. In *19th AIAA/CEAS Aeroacoustics Conference*, AIAA Paper 2013-2105, Berlin, Germany, June 2013b.

M. Sturm and T. Carolus. Unsteadiness of blade-passing frequency tones of axial fans. In *21st International Congress of Sound and Vibration*, No. 248, pages 1440–1500, July 2014.